Int. J. Heat Mass Transfer. Vol. 18, pp. 415–431. Pergamon Press 1975. Printed in Great Britain

ON THE BUOYANCY-INDUCED FLOW ARISING FROM A HEATED HEMISPHERE

YOGESH JALURIA* and BENJAMIN GEBHART
Sibley School of Mechanical and Aerospace Engineering, Upson Hall, Cornell University, Ithaca, NY 14850, U.S.A.

(*Received* 31 *May* 1974)

Abstract—An experimental study of the natural convection flow over heated hemispheres has been carried out. The boundary-layer flow adjacent to the heated surface and the buoyant flow shed above it were studied in detail. Both the upright and inverted hemisphere configurations were considered to determine the effect on the resulting flow for the two characteristic orientations. Of major interest was the way in which the heated fluid adjacent to the surface rises from it and develops into a buoyant plume above the body. Detailed measurements of the velocity and temperature fields in regions close to the top of the hemisphere were made. The measured plume flow is compared with the axisymmetric plume which would rise above a point heat source. Local and average heat-transfer rates were determined. Our measurements in the boundary region upstream of the trailing end of the hemisphere also enable us to consider further the concept of "separation" in natural convection in greater detail than heretofore. It is found that the upright hemisphere generates higher velocities and a thicker boundary region than does the inverted orientation. The average heat-transfer rate is also greater. Plume flow was also measured above an inclined hemisphere. The effect of an extended insulator base under the upright hemisphere was determined. Two surface boundary conditions, uniform temperature and uniform heat flux, were studied and hemispheres of two sizes were used. Our measurements are found to be in reasonable general agreement with existing theoretical and experimental results for spheres. These results clarify many fundamental questions concerning the nature of separation in natural convection and the effect of buoyancy force orientation and of surface geometry on flow over curved surfaces. The collection of the shed boundary region fluid into a buoyant plume is an interesting and varied process.

NOMENCLATURE

C_p, specific heat at constant pressure of the fluid [cal/g°C];
d, vertical distance in plume flow [cm];
D, diameter of the hemisphere [cm];
g, acceleration due to gravity [cm/s^2];
Gr, Grashof number, $Gr = \dfrac{g\beta D^3 \Delta T}{\nu^2}$;
h, local heat-transfer coefficient [cal/cm^{2}s°C];
$\bar{h}$, average heat-transfer coefficient [cal/cm^{2}s°C];
k, thermal conductivity of the fluid [cal/cm s°C];
K_1, Prandtl number dependent constant in equation (1);
K_2, Prandtl number dependent constant in equation (2);
Nu, local Nusselt number, $Nu = \dfrac{hD}{k}$;
$\overline{Nu}$, average Nusselt number, $\overline{Nu} = \dfrac{\bar{h}D}{k}$;
Pr, Prandtl number of the fluid, $Pr = \dfrac{\nu}{\alpha}$;
q, local surface heat flux [W/m^2];
q'', surface heat flux for uniform flux condition [W/m^2];
Q, total heat input by the hemisphere [W];
r, radial distance out from hemisphere surface [cm];
Ra, Rayleigh number, $Ra = Gr.Pr$;
t, measured local temperature [°C];
t_0, measured surface temperature, also centreline temperature in plume flow [°C];
t_∞, temperature of ambient medium [°C];
ΔT, surface temperature difference from ambient [°C];
U_m, measured physical velocity [cm/s];
U, nondimensional velocity;
V, measured upward velocity in plume flow [cm/s];
x, distance above a concentrated heat source [cm];
y, horizontal distance from the centerline in plume flow [cm].

Greek symbols

α, thermal diffusivity of the fluid [cm^2/s];
β, coefficient of thermal expansion of the fluid [°C^{-1}];

* Present address: Engineering Research Center, Western Electric Co., P.O. Box 900, Princeton, NJ08540, U.S.A.

η, nondimensional radial distance in boundary layer;

δ_v, nondimensional velocity boundary-layer thickness;

δ_T, nondimensional thermal boundary-layer thickness;

ν, kinematic viscosity of the fluid [cm^2/s];

ϕ, dimensionless temperature, $\phi = \dfrac{t - t_\infty}{t_0 - t_\infty}$;

ρ, density of fluid [g/cm^3];

θ, angular downstream location, Fig. 1 [degrees].

INTRODUCTION

IN STUDIES of natural convection transport, we frequently encounter a boundary-region flow adjacent to a heated curved surface. The heated fluid ultimately leaves the surface and rises above the body as a buoyancy-driven plume. Two important flow configurations arise, depending on whether the component of the buoyancy force normal to the surface is directed away from or toward it. This study concerns the nature of the transport processes around an "incomplete" surface, at different orientations, and the eventual separation into a buoyant plume.

The flow was generated by a heated hemisphere in an extensive isothermal medium. Upright, inverted and inclined orientations were studied. Velocity and temperature distributions were measured near the surface and in the resulting plume flow.

Considerable work has been done on the natural convection flow over heated spheres. However, there has been no study of hemispherical surfaces, even though this configuration, or one similar to it, is often encountered. Moreover, few detailed measurements of the velocity and temperature field in the boundary region over the spherical surface have been taken. No quantitative study of the way the plume is formed, or of its later flow, has been made. The major emphasis has been on the local and overall heat-transfer rates. Recently, Amato and Tien [1] studied the flow and heat-transfer characteristics of heated spheres in water. The ambient temperature was varied, providing a range of Prandtl number, Pr. A correlation of their overall heat-transfer rates was compared with the results of other investigations. Local heat-transfer rates were determined from the slope of measured temperature profiles, at the wall. However, they did not make a detailed study of the boundary region at downstream locations far enough from the stagnation point of the sphere to study the development of the boundary region flow into the shed plume. The sphere surface at the top was encumbered by a support tube. No measurements were made in the shed plume.

Kranse and Schenk [2] measured local and overall heat-transfer rates from an isothermal sphere in benzene, $Pr = 8{\cdot}3$. An attempt was made to interpret a region where the boundary layer separated, in terms of the variation of the local heat-transfer rate along the sphere surface. Similar studies, of mass transfer, were made by Schutz [3] and Garner and Keey [4].

There has been some analysis of boundary-region flow over the surface of a heated sphere. Merk and Prins [5] pointed out that a similar solution is not obtainable and employed an integral method to estimate heat-transfer rates and velocity profiles, for a wide range of Pr. Acrivos [6] considered heat transfer for $Pr \to \infty$. Chiang *et al.* [7] used a series method to obtain velocity and temperature profiles and heat-transfer rates for $Pr = 0{\cdot}7$. Braun *et al.* [8] assessed similarity for bodies with closed lower ends and discussed the extension of their results to nonsimilar bodies.

It is evident that, though some comparison with the existing work is possible for our measurements on the inverted hemisphere, as the bottom half of a sphere, almost no information is available for the upright hemisphere or for the eventual plume flow. Our purpose was to measure in detail the flow and temperature distributions both in the boundary region adjacent to a heated hemisphere and in the freely rising plume above it. Of major interest was the flow near the top of the hemisphere, where the boundary region flow develops into the shed plume. We were also interested in any "separation" of the boundary layer preceding this development into a plume. The velocity and temperature fields in regions close to the top were, therefore, studied in detail.

Our studies were carried out on heated hemispheres in water, $Pr = 7{\cdot}0$, at two surface conditions, uniform temperature and uniform heat flux. The measurements of velocity and temperature led to many interesting conclusions regarding the flow near the top of an upright hemisphere, where the boundary layers from all sides meet and rise in a single concentrated plume. Heat-transfer rates, local and overall, were determined from the electrical input to the individual heaters. We found a substantial difference in the flow fields for the two orientations of the hemisphere, inverted and upright.

We also made measurements of the plume flow above an inclined hemisphere, with a uniform surface heat flux, to determine the nature of the flow and departure from symmetry. Measurements were also made for an upright hemisphere seated on an extensive insulator surface. Such heated bodies are frequently situated on unheated, or neutral, surfaces. We wanted to determine the resulting effect, if any, on the heat-transfer rate and flow.

All of our measurements indicated a gradual thickening of the boundary layer and an increase in the tangential velocity downstream, around the curved surface, from the leading edge in the upright case and from the stagnation point in the inverted one. In the inverted configuration, the heat-transfer coefficient, h, decreased all the way to the trailing edge. For the upright hemisphere, a rapid thickening of the boundary region and a sharp increase in the velocity was observed near the top. The heat-transfer coefficient decreased with θ to a minimum and it then showed a sharp increase near the top of the surface, indicating that a strong effect was induced in the formation, or shedding, of the plume.

Measurements in the plume indicated a velocity and temperature field close to that determined theoretically for an axisymmetric plume formed above a point heat source and an attempt is made to relate the two. Some measurements were also made in the wake behind the inverted hemisphere. The presence of an insulator base surface was found to decrease the velocity level and increase the boundary region thickness. This suggests a lower-heat-transfer coefficient, which we found.

We also measured the surface temperature variation for a uniform surface heat flux condition. Hemispheres of 15·2 and 30·5 cm dia were studied to evaluate any scale effect in our experiment. No appreciable effect was observed. A comparison of our measurements with the existing theoretical and experimental results indicated a good agreement.

EXPERIMENTAL ARRANGEMENT

The experiment was carried out in water, $Pr = 7{\cdot}0$. Two hemisphere sizes, of O.D. 15·2 and 30·5 cm, were employed. Both were of aluminum with a wall thickness of approximately 2 mm. The surface was anodized for resistance to corrosion by water.

The hemispheres were heated by means of several flexible heating tapes bonded to the inside surface with high temperature cement. Each tape was about 2·8 cm wide. The heaters were placed circumferentially in planes parallel to the hemisphere base. This ensures axisymmetry of flow when the hemisphere base is horizontal. Eight separate heater tapes were employed to heat the bigger hemisphere and four for the smaller one, approximately covering the entire inner surface. The electrical input to each heater was individually controlled by variable resistances in series. Voltages were measured by a digital voltmeter and the current by a standard shunt resistance in series. The power input to each heater was determined.

The surface temperature for the larger hemisphere was determined by means of fourteen copper–constantan thermocouples of $1{\cdot}27 \times 10^{-2}$ cm dia. The thermocouple junctions were placed midway through the hemisphere wall, in small holes drilled from the inside, and were embedded in epoxy resin. One thermocouple junction was located near the centerline of each of the eight heaters. The remaining six thermocouples were placed at various other positions to serve as a check for the uniformity of surface temperature. A similar arrangement was used for the smaller hemisphere.

A uniform temperature on the hemisphere surface was achieved by adjusting the power input to the individual heaters. Due to the axisymmetric positioning of heaters, uniform surface temperature is assured only when the hemisphere base is horizontal. However, if all the heaters are put in series, the uniform surface heat flux condition is achieved, for heaters of uniform resistance per unit length and negligible wall conduction. Approximate calculations indicated that conduction would not cause a deviation of greater than 10 per cent from the uniform flux condition. This surface condition was employed for some measurements. By adjusting the input to the independent heaters, all the thermocouples at the heaters could easily be brought to within 0·05°C of each other, to attain the isothermal condition. The remaining thermocouples also indicated temperature uniformity within a few per cent of the mean.

A regulated d.c. power supply, Nobatron MR36–30, capable of providing up to 36 V and 30 A, supplied the heaters, which, with resistances in series, were connected in parallel across the power supply. The variable resistances were varied to make the hemisphere surface isothermal and the local heat flux was obtained from the individual power inputs.

The investigation was conducted in a $61 \times 61 \times 73$ cm high insulated stainless steel tank with circular plexiglass windows of 20·3 cm dia. The top of the hemisphere was about 32 cm below the water surface and was visible through the windows. Flow near the trailing end of the hemisphere was visualized by Schlieren. The water purification system described by Hollasch [9] was used to keep the water free of suspended impurities and ions, a necessary condition for the use of bare hot wires. The tank was filled with distilled water and the purification system was used to raise the resistivity level of the water to above 1 MΩ cm. Purification at regular intervals and isolation of the water from dust and other particles outside by means of teflon sheets placed on the water surface enabled us to preserve this purity.

Hemispheres were positioned in the tank by a stainless steel support capable of horizontal and vertical adjustment. The hemispheres were assembled as follows. After the bonding of the heaters and the thermocouples, the hemisphere was filled with Urethane insta-foam. The base of the hemisphere was then closed by a circular 3-mm thick plexiglass plate, insulated on

the outside. A plexiglass tube of 4·5 cm dia and 3 mm wall thickness was attached normal to the base, at the center. Connections from the heaters and the thermocouples were passed through it. For the study of the upright hemisphere with an extended insulator base, the hemisphere was attached to a styrofoam insulator sheet which was in turn fixed to the support. Proper orientation in all studies was determined with a plumb bob and a level.

Measurements of the flow velocity were made with a constant temperature hot wire anemometer (DISA Model 55D01). The single sensor was always horizontal and at right angles to the direction of traverse, which was radial for measurements adjacent to the surface and horizontal and radial for those in the plume. The hot wire essentially measures the velocity component at right angles to the sensor. The hot wire supports were silver plated and the sensor wire was of $1{\cdot}27 \times 10^{-3}$ cm dia platinum. The hot wire overheat ratio of 1·1 employed resulted in a sensor temperature excess of about 33°C above the ambient. For further details on hot wire calibration and velocity measurement, see Jaluria and Gebhart [10].

The temperature measurements in the flow field were made by means of a $1{\cdot}27 \times 10^{-2}$ cm dia copper–constantan thermocouple located adjacent to the hot wire probe and attached to its support. A similar thermocouple was placed in the ambient medium at one end of the tank. This thermocouple had a reference junction at 0°C (ice point) and it, therefore, measured any temperature changes in the tank. All thermocouples in the hemisphere had the ambient thermocouple as reference and, therefore, the temperature difference from the ambient was obtained directly.

A mechanism for traversing in the vertical, horizontal and transverse directions was employed to position the hot wire probe and thermocouple at any location in the flow field. The position in the three directions was measured by micrometers with divisions of 0·025 mm. The position of the surface was determined locally by means of an auxiliary electrical circuit.

The hot wire and thermocouple signals were simultaneously recorded on two channels of an Offner Dynograph (Type R). The highest sensitivity of the recorder was 10 μV/cm, which gives a temperature sensitivity of about 0·22°C/cm. The signals from the thermocouples inside the hemisphere were measured with a digital voltmeter (Dana 4800) whose least count was 1 μV.

Due to the good thermal response of the heaters and the thinness of the hemisphere wall, steady flow was attained within about 15 min. Test times of the order of 30 min could be used, for most of the heating rates employed, without causing appreciable stratification in the tank. Since the surface temperature was usually only a few degrees above the ambient, fluid property variations were ignored. To check the accuracy and repeatability of our measurements, several experiments were repeated. Our data showed a reproducibility within about 5 per cent for the velocity, temperature and heat-transfer rates.

EXPERIMENTAL RESULTS

For our flow circumstance, in which the surface temperature is higher than the ambient temperature, the coordinate system is as shown in Fig. 1. The

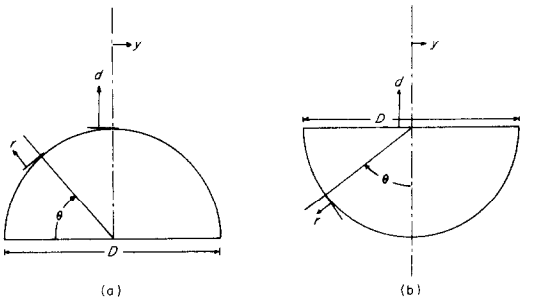

FIG. 1. Definition of the coordinate system: (a) Upright, (b) Inverted.

downstream location along the surface is given in terms of θ, the angle from the stagnation point for the inverted hemisphere and from the circular leading edge for the upright case. The radial distance out from the surface is r. For the downstream plume, d and y are the vertical and horizontal coordinates. In the upright position, the axis of the hemisphere coincides with the vertical direction. However, in the inclined position, the axis moves away from the vertical and d is measured along the radial direction coinciding with the vertical.

1. *Boundary region flow, adjacent to the heated surface*

Our results for the isothermal surface condition are best compared with others in terms of the following non-dimensionalization. See, for example, the analysis of Merk and Prins [5].

$$\eta = \frac{r}{D} Gr^{1/4} \quad \text{and} \quad U = U_m \Big/ \left(\frac{\nu}{D} Gr^{1/2} \right)$$

with

$$Gr = \frac{g\beta D^3 \Delta T}{\nu^2}$$

where D is the diameter of the hemisphere, U_m the measured physical velocity, ν the kinematic viscosity, β the coefficient of thermal expansion, ΔT the surface temperature difference from the ambient, g the acceleration due to gravity and Gr the Grashof number.

Inverted hemisphere. Since some theoretical and experimental information exists for boundary region flow

over a sphere, we shall first present our results for the inverted hemisphere, which may resemble the lower half of a complete sphere. The measured velocity profiles, at $\theta = 30°, 45°, 60°$ and $75°$, are shown in Fig. 2

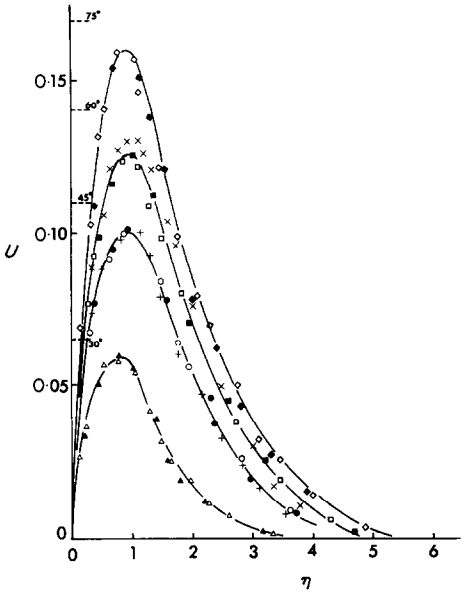

FIG. 2. Velocity distributions in the boundary region over the inverted hemisphere at various downstream locations θ. Data: $D = 30{\cdot}5$ cm, $Ra = 6{\cdot}9 \times 10^8$; △, $\theta = 30°$; ○, $\theta = 45°$; □, $\theta = 60°$; ◇, $\theta = 75°$. $D = 30{\cdot}5$ cm, $Ra = 15{\cdot}5 \times 10^8$; ▲, $\theta = 30°$; ●, $\theta = 45°$; ■, $\theta = 60°$; ◆, $\theta = 75°$. $D = 15{\cdot}2$ cm, $Ra = 0{\cdot}86 \times 10^8$; +, $\theta = 45°$; ×, $\theta = 60°$.

for the two diameters, 15·2 and 30·5 cm, at two heating rates for the latter. Note that the Rayleigh number $Ra = GrPr$.

The velocity increases rapidly downstream and the profile changes in form, the peak remaining at about $\eta = 1$ as the layer thickens. Both effects indicate extreme nonsimilar behaviour, in terms of U and η. At each location θ, however, the theory predicts a correlation in terms of these variables, see, for example, Chiang *et al.* [7]. The two sets of data for $D = 30{\cdot}5$, at different heating rates, confirm this prediction. Also shown are data at $\theta = 60°$ and 45° for the smaller hemisphere at $Ra = 0{\cdot}86 \times 10^8$. These results, at the same temperature difference as for the larger hemisphere at $Ra = 6{\cdot}9 \times 10^8$, also correlate well.

Thus, although η and U correlate at each θ, over the range of our data, they fail to give similarity since the profiles vary downstream with θ. This result of heat addition and of entrainment of ambient fluid was estimated by Merk and Prins [5] as a function of Pr and the angular position θ. Their values of U_{max}, interpolated for $Pr = 7{\cdot}0$, are shown along the vertical axis of Fig. 2. Our measurements are around 10 per cent lower, which is not surprising given the approximate nature of the analysis and an undetermined error in our interpolation. Amato and Tien [1] measured U_{max} 14·6 per cent lower than the predicted value at $\theta = 45°$. The gradual outward shift of the location of maximum velocity agrees with the calculated profiles of Chiang *et al.* [7], for $Pr = 0{\cdot}7$. This shift is expected from the thickening of the boundary region.

Temperature profiles for 30·5 cm dia and one heating rate, $Ra = 6{\cdot}9 \times 10^8$, are shown in Fig. 3 in terms of

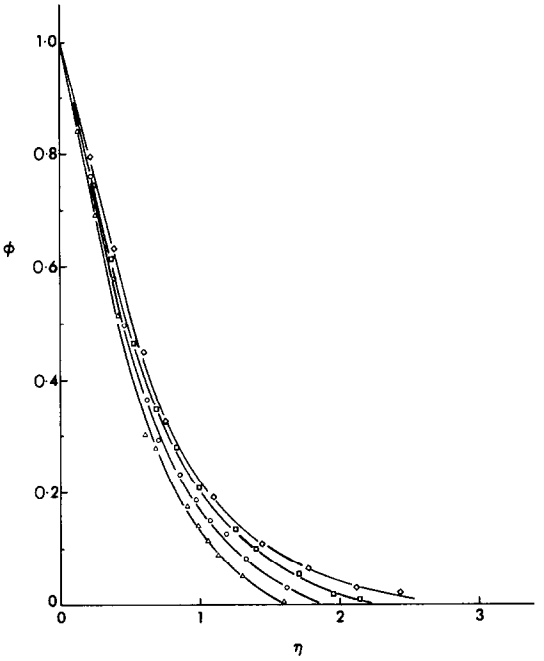

FIG. 3. Temperature distributions in the boundary region over the inverted hemisphere at $Ra = 6{\cdot}9 \times 10^8$ and at various values of θ. $D = 30{\cdot}5$ cm. Data: △, $\theta = 30°$; ○, $\theta = 45°$; □, $\theta = 60°$; ◇, $\theta = 75°$.

$\phi = (t - t_\infty)/(t_0 - t_\infty)$, where t is the measured local temperature, t_0 is the surface temperature and t_∞ is the temperature of the ambient medium. Data for $D = 15{\cdot}2$ cm at $Ra = 15{\cdot}5 \times 10^8$, though not shown, are very similar at each θ. These ϕ curves agree in form with the measurements of Amato and Tien [1] and the calculations of Chiang *et al.* [7]. The slope at the wall gradually decreases downstream indicating a corresponding decrease in the local heat-transfer rate. The thermal layer thickens, but remains much thinner than the velocity layer. The growth of both the velocity and temperature layers is considered in greater detail later.

Upright hemisphere. In this configuration, the buoyancy force is directed increasingly away from the surface

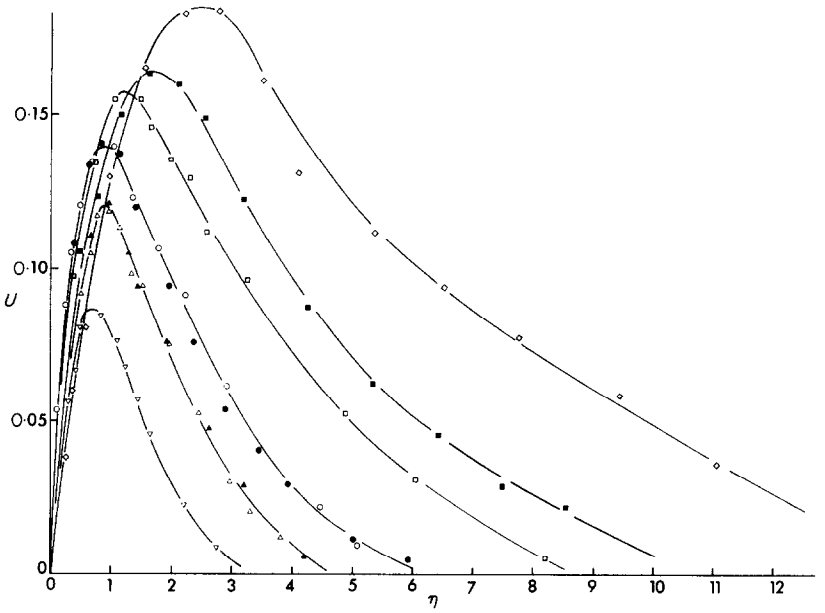

FIG. 4. Velocity distributions for the upright configuration at various values of θ, $D = 30{\cdot}5$ cm. Data: $Ra = 6{\cdot}9 \times 10^8$; $\nabla, \theta = 15°$; $\Delta, \theta = 30°$; $\bigcirc, \theta = 45°$; $\square, \theta = 60°$; $\diamond, \theta = 75°$. $Ra = 20{\cdot}4 \times 10^8$; $\blacktriangle, \theta = 30°$; $\bullet, \theta = 45°$; $\blacksquare, \theta = 60°$.

at larger θ and the flow periphery rapidly decreases near the top. Both effects suggest significant differences in the boundary region flow and heat transfer from the inverted case.

The distributions of U vs η in Fig. 4 are very different from those measured in the inverted position. At each θ the maximum value of U is larger and the boundary layer appreciably thicker. Since the buoyancy force component normal to the surface is now outward the boundary-layer thickness increases. In addition, the tangential component of the buoyancy force in the region of the leading edge of the flow is much larger, causing early acceleration. Also, the decreasing body cross section downstream decreases the peripheral length of the boundary region. The resultant and increasing circumferential piling of the fluid would certainly thicken the boundary layer and possibly also contribute to higher velocities. The resulting effect on heat transfer is discussed later.

The behavior of the flow near the top is very interesting. The distributions for the two heating rates coincide up to $\theta = 45°$. However, at $\theta = 60°$, the boundary region is thicker and peak velocity higher for the higher heating rate. This characteristic is seen more sharply in Fig. 5 where we plot the downstream (θ) variation of the velocity and temperature boundary layer thickness. The edge of the velocity layer δ_v is defined as the η location where the velocity has dropped to 5 per cent of its local maximum value. With this definition, the values of δ_v may be obtained accurately

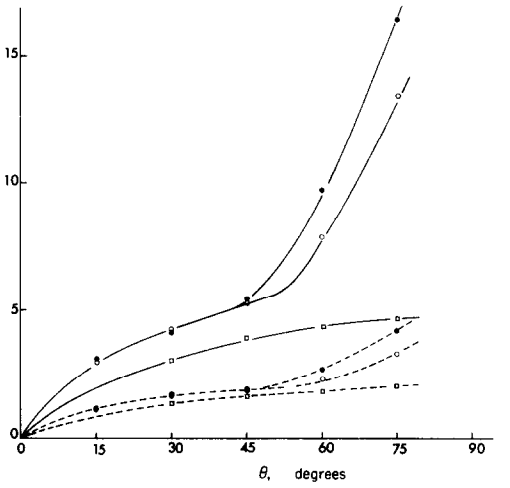

FIG. 5. Growth of boundary layer thickness δ, with θ, ——, velocity (δ_v) and – – –, temperature (δ_T). $D = 30{\cdot}5$ cm. Data: ○, Upright at $Ra = 6{\cdot}9 \times 10^8$; ●, Upright at $Ra = 20{\cdot}4 \times 10^8$; □, Inverted at $Ra = 6{\cdot}9 \times 10^8$.

even for profiles which are very flat at large η. The edge of temperature boundary layer δ_T is similarly defined as the η location where $\phi = 0{\cdot}05$. We see that both the magnitude of each boundary-layer thickness and their growth with θ are independent of the heating rate, up to around 45°. Then the growth rates abruptly become greater for the higher heating rate. At the lower heating rate the abrupt change occurs at larger θ. For the inverted hemisphere, the initial behavior is strikingly

similar, at appreciably smaller local thickness, but the sudden increase in growth rate does not occur.

These flow characteristics, at larger θ, lead to the question of "separation". Also, it is obvious that something dramatic must happen at larger θ to collect all of the fluid and redirect it strictly upward. The experimental study of Pera and Gebhart [11], on a cylindrical surface, has shown that the usual phenomenon of "flow separation", with backflow, does not take place and is not the mechanism in such natural convection flows. The flow does separate from the surface as the boundary-layer material from all sides meets at the top. But this is not due to a first-order interaction with an external pressure field. Nor is it now found to result in flow reversal downstream of separation. The heated fluid is, apparently, simply realigned upward and rises in a steady, developing and axisymmetric buoyant plume.

Since the flow rate in the boundary layer over the surface is appreciable, the realignment must begin well ahead of the topmost point, resulting in the abrupt change in boundary-layer thickness growth rate. The location, in θ, at which this occurs may, perhaps, be assumed to be the beginning of the region wherein the heated fluid has developed an appreciable normal velocity component, as the tangential one decreases downstream to become zero at the axis of symmetry.

Our hot wire was actually measuring the magnitude of the component of the velocity vector normal to itself and that is what is plotted, e.g. in Fig. 4. The local maxima are replotted in Fig. 6, vs θ. The initial downstream increase is similar in form to that for a flat vertical surface, which is shown for comparison. The increased acceleration at around 45° for the larger heating rate, and around 60° for the smaller, is the evidence of the same effect as that discussed earlier in terms of boundary region thickness. This deviation is more gradual than that of δ_v and it is first apparent somewhat further downstream. However, either distribution might be employed as a measure of the location where boundary region material starts rising from the heated surface. An initial rapid downstream decrease in the heat-transfer coefficient h at this location is suggested by a sharp increase in boundary-layer thickness upstream of the rapid rise in velocity.

On Figs. 5 and 6 we also see the results for the inverted orientation. Clearly both quantities, boundary-layer thickness δ (δ_v or δ_T) and U_{max}, increase regularly with θ, there is no sudden change in trend. This difference indicates the profound differences between the two orientations, which will also be apparent in heat-transfer behavior.

Measured temperature profiles for the larger hemisphere, upright, are shown in Fig. 7, at $Ra = 6{\cdot}9 \times 10^8$. The thermal boundary layer also thickens downstream. However, the slope at the wall first decreases in magnitude, to about $\theta = 60°$, and then has greatly increased again by $\theta = 75°$. The local heat transfer, proportional to $[-\phi'(0)]$, has gone through a minimum value. Similar behavior was observed for the higher heating rate and for the smaller hemisphere.

We also made measurements with the large hemi-

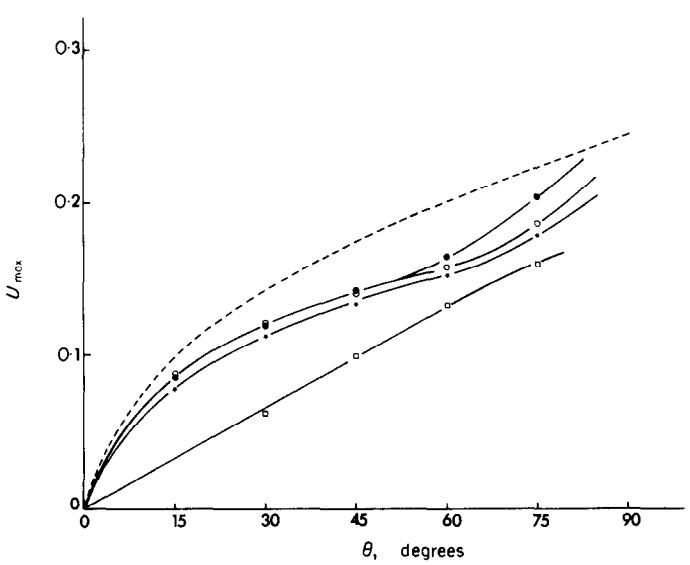

FIG. 6. Variation of maximum velocity U_{max}, with θ. $D = 30{\cdot}5$ cm. ----, Vertical surface at same ΔT as at $Ra = 6{\cdot}9 \times 10^8$. Data: ○, Upright at $Ra = 6{\cdot}9 \times 10^8$; ●, Upright at $Ra = 20{\cdot}4 \times 10^8$; □, Inverted at $Ra = 6{\cdot}9 \times 10^8$; ★, Upright with extended insulator base at $Ra = 6{\cdot}9 \times 10^8$.

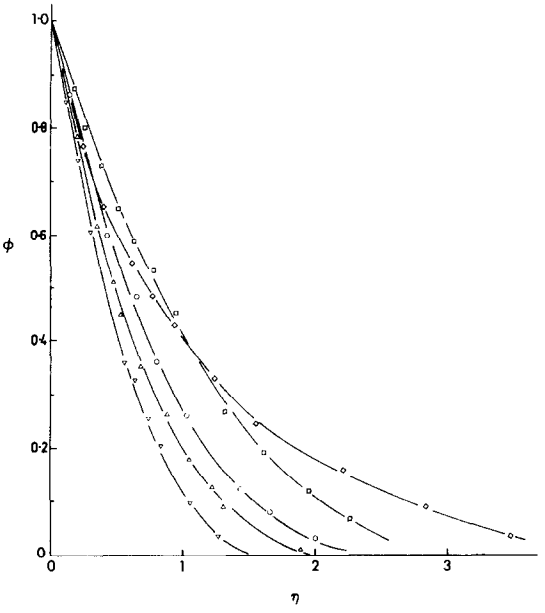

FIG. 7. Temperature distributions in the boundary region, upright hemisphere at $Ra = 6{\cdot}9 \times 10^8$ and at various values of θ. $D = 30{\cdot}5$ cm. Data: ∇, $\theta = 15°$; $\triangle$, $\theta = 30°$; $\bigcirc$, $\theta = 45°$; $\square$, $\theta = 60°$; $\diamond$, $\theta = 75°$.

sphere seated on an extended insulator base. This configuration is more appropriate to applications. The velocity profiles at $Ra = 6{\cdot}9 \times 10^8$, are shown in Fig. 8. A comparison with the results without the base, in Fig. 4, indicates that the velocity boundary layer is about 20 per cent thicker and that the local velocity maxima are about 5 per cent less. Both effects tend to lower the local heat-transfer rate for a given ΔT. The magnitude of $-\phi'(0)$ was found to be 10–15 per cent lower. Therefore, except for level, we conclude that the two configurations give similar results.

The changes may be explained by the effect of the insulator base cutting out any induction of flow from below. This reduction in the supply of fluid requires greater entrainment from the side, which gives rise to a thicker boundary layer in regions close to the leading edge. Both the local heat transfer and flow rate are reduced. This effect persists downstream, giving rise to thicker boundary regions, lower heat-transfer rates and a slightly lower velocity level.

2. *Heat transfer*

The temperature profiles indicate the expected θ variation of the local heat-transfer rate. The heat-transfer rates, both local and overall, were also determined directly from the energy input to the heaters and the measured temperature difference. These results are presented in terms of the local Nusselt number, $Nu = hD/k$, and the overall Nusselt number, $\overline{Nu} = \bar{h}D/k$, where h is the local heat-transfer coefficient, $\bar{h}$ is its average value and k is the thermal conductivity of water. The heat-transfer coefficient h is given by $h = q/\Delta T$, where q is local surface heat flux calculated from the

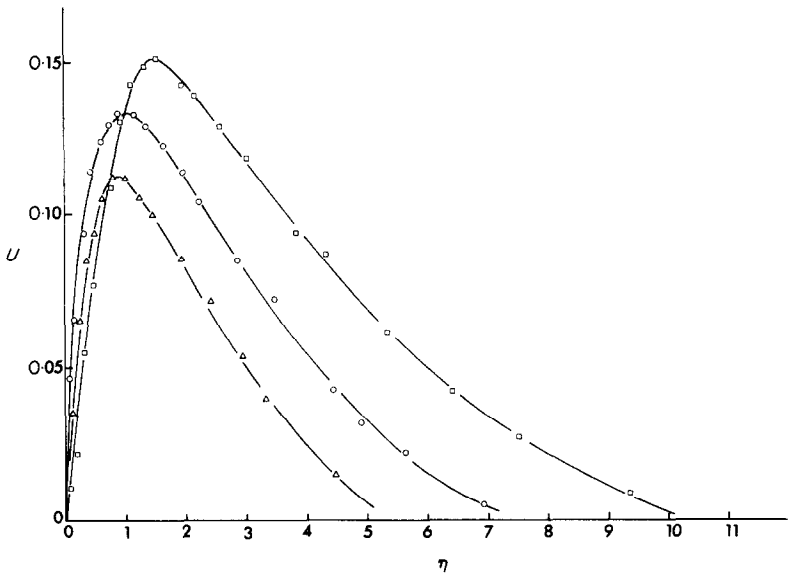

FIG. 8. Velocity distributions in the boundary region, upright hemisphere with extended insulator base at $Ra = 6{\cdot}9 \times 10^8$ and at various values of θ. $D = 30{\cdot}5$ cm. Data: $\triangle$, $\theta = 30°$; $\bigcirc$, $\theta = 45°$; $\square$, $\theta = 60°$.

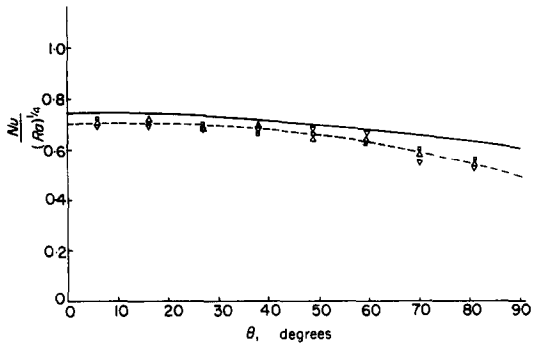

FIG. 9. Variation of the local heat-transfer coefficient h with θ for the inverted configuration. $D = 30{\cdot}5$ cm. ——, prediction from Merk and Prins [5]. Data: □, $Ra = 2{\cdot}15 \times 10^8$; △, $Ra = 5{\cdot}74 \times 10^8$; ▽, $Ra = 19{\cdot}2 \times 10^8$.

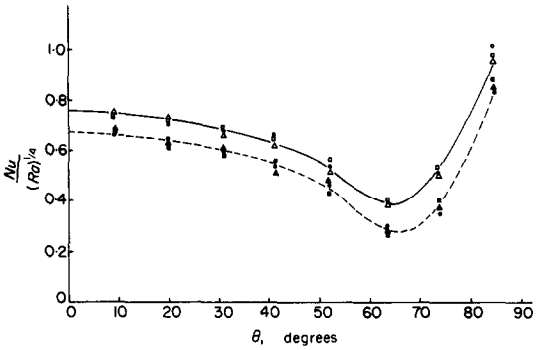

FIG. 10. Variation of the local heat-transfer coefficient h with θ for the upright configurations. $D = 30{\cdot}5$ cm. Data: Without base; ○, $Ra = 2{\cdot}1 \times 10^8$; △, $Ra = 12{\cdot}1 \times 10^8$; □, $Ra = 17{\cdot}4 \times 10^8$. With base; ●, $Ra = 5{\cdot}05 \times 10^8$; ▲, $Ra = 12{\cdot}6 \times 10^8$; ■, $Ra = 20{\cdot}4 \times 10^8$.

power input to individual heaters and the area each supplies at the outer surface. Similarly $\bar{h}$ is based on the total input to the heaters and the total surface area. The results are shown in Figs. 9–11 in terms of Nu and $\overline{Nu}$, normalized by $(Ra)^{1/4}$.

The local variation is seen in Fig. 9 for the inverted 30·5 cm hemisphere, along with the prediction of Merk and Prins [5] interpolated to $Pr = 7{\cdot}0$. Our data, at three values of Ra covering the range of our measurements, are very close to each other, indicating a good correlation with $(Ra)^{1/4}$. The single curve of their trend is close to the theory, being about 5 per cent less at $\theta = 0°$ and increasing to almost 20 per cent less at $\theta = 90°$. Recall that our measured velocity maxima were about 10 per cent lower than the predicted ones. Data for the $D = 15{\cdot}2$ cm hemisphere were found to be similar. Kranse and Schenk [2] also measured the variation of $Nu/(Ra)^{1/4}$ with θ. Most of their experimental results are 10–20 per cent lower than those calculated.

Our results for the upright hemisphere, with and without the insulator base, are shown in Fig. 9 for three different heating rates for each. For each configuration $(Ra)^{1/4}$ again correlates the data. However, these results are very different from those in Fig. 9. Although in both orientations there is a slow initial decrease with increasing θ, this data descends more rapidly to a minimum at around $\theta = 60°$. Thereafter, unlike the inverted orientation, the heat-transfer parameter rises sharply to very high values. Kranse and Schenk [2] observed a similar behavior of the local heat-transfer coefficient near the top of heated spheres. A similar effect was noted in the mass-transfer studies of Garner and Keey [4] and Schutz [3]. The location of the

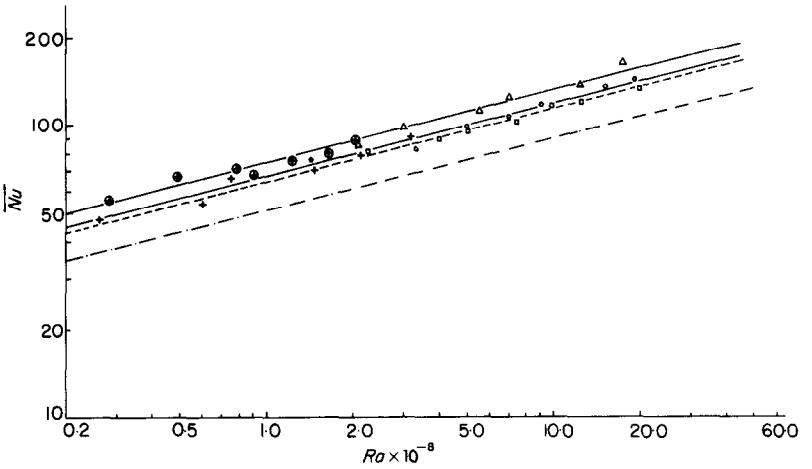

FIG. 11. Variation of average heat-transfer coefficient $\bar{h}$ with θ. —·—, correlating curve for sphere, Amato and Tien [1]. Data: $D = 30{\cdot}5$ cm; △, upright without base; □, upright with base; ○, inverted. $D = 15{\cdot}2$ cm; ⊕, upright without base; +, inverted.

minimum was called the "separation" point by Kranse and Schenk [2].

It is clear from our former data that the increase in heat transfer beyond the minimum is a consequence of changing boundary-layer behavior near the top of the hemisphere. The transition of the flow into a buoyant plume above the hemisphere results in a sharp increase in local flow velocity and of boundary-layer thickness. The rapid increase in velocity causes the increase in heat transfer in spite of increasing boundary-layer thickness, which usually reduces the local heat-transfer parameter.

Our data does show that the initial effect of an increase in velocity is somewhat offset by the effects of increased boundary-layer thickness. The minimum heat-transfer coefficient occurs well downstream of the first severe deviation in δ and U_{max} from their upstream trends, see Figs. 5 and 6. It is interesting that, although the deviations in U_{max} and δ depend sharply on Ra, the heat-transfer coefficient minimum does not. In fact, the minimum is quite flat, making an estimation of its exact location difficult. This agrees with the observations of Kranse and Schenk [2]. Recall that our U_{max} and δ variations with θ indicate that the boundary layer begins rising at lower θ for higher Ra. This observation is supported by the conclusions of Garner and Keey [4] and Schutz [3]. Incidently, this effect will presumably give rise to initially thicker plumes at higher Ra. We note that Fig. 10 also shows a somewhat lower heat-transfer coefficient $\bar{h}$ at given Ra for the hemisphere with an insulator base, in accordance with our earlier discussion.

Our average heat-transfer results are plotted in Fig. 11 over a large range of heating rate, Ra, for all three configurations. The collection of data has considerable spread. Nevertheless, the average trend of $\overline{Nu}$ is approximately as $(Ra)^{1/4}$ and the data for the two hemisphere sizes, for each orientation, are not significantly different. The experimental curve obtained by Amato and Tien [1], for heat transfer from isothermal spheres in water, is shown for comparison.

The upright hemisphere, without the base, has the largest $\overline{Nu}$ at given Ra. With the base it is about 15 per cent lower. Recalling the low minimum in Nu for the upright hemisphere, Fig. 10, it seems initially surprising that its average heat-transfer coefficient at given ΔT is greater than for the inverted hemisphere, for which h drops more gradually with θ. However, the body cross-section changes downstream in a different way for the two orientations. When inverted, the greatest contribution to the average comes at large θ, where the value of h has dropped considerably. When upright, the largest contribution comes at low values of θ, where h is large. Also the value of h at small θ is larger for the upright case because the velocity is.

It is also noted from Fig. 11 that the average Nusselt number $\overline{Nu}$ is higher for the inverted hemisphere than that measured for the whole sphere at the same Ra. Thus, we would infer, that for a heated sphere, the heat transfer from the bottom half is greater than that from the upper half. This is expected from the continued decrease in h with θ over the major part of the surface on the upper half of the sphere, see Merk and Prins [5]. At the very start of the upper half, $\theta = 90°$, h has already decreased substantially from its highest value at the stagnation point, $\theta = 0°$. This is reflected in a lower average heat-transfer coefficient for the upper half of a heated sphere.

3. *Plume flow*

We also made a detailed investigation of the buoyant flow above the upright hemisphere. We were particularly interested in the region close to the top of the hemisphere and in the adjustment of the flow downstream into the plume, i.e. in the interaction region. Since the flow adjacent to the surface was axisymmetric, the flow above it is also expected to be axisymmetric. We were, therefore, interested in comparing our measurements with the predictions of the analysis of a laminar axisymmetric plume flow arising from a point heat source. We also wished to determine the local regime, laminar, transition or turbulent, of the plume flow and to observe any instability to naturally occurring disturbances.

We measured the velocity and temperature distributions at several downstream locations d. For the range of Ra and d investigated, the plume flow above the hemisphere was found to be laminar. However, for the 30·5 cm hemisphere, and for $Ra = 20{\cdot}4 \times 10^8$, we did observe the presence of amplified disturbances, at and beyond $d = 15{\cdot}2$ cm. These disturbances were found to be closely sinusoidal. Their frequency and amplitude were determined. These results are considered, in light of existing information on the stability of natural convection flows, later in this section.

Measured profiles of the upward velocity V at various distances d above the upright hemispheres, without the base, are shown in Fig. 12. The distributions were found to be symmetric about the axis and are shown for only one side. Note that the values of d are of the same order as the flow region diameter so that this is the interaction region.

The most detailed data, for $D = 30{\cdot}5$ cm and $Ra = 6{\cdot}9 \times 10^8$, indicate that the diameter of the flow region first decreases very rapidly and then begins to increase again, as in a plume, as the fluid is gathered into a more orderly motion. The minimum diameter occurs at around $d = 10{\cdot}2$ cm. The maximum velocity increases downstream and the distributions indicate that the plume flow rate also increases rapidly, by entrain-

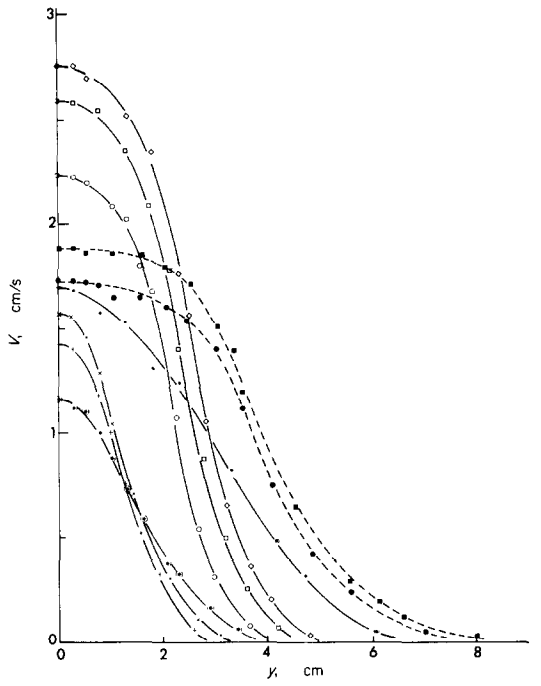

FIG. 12. Velocity distributions in the plume above the upright hemispheres, at various d. Data: $D = 30{\cdot}5$ cm, $Ra = 6{\cdot}9 \times 10^8$; ◉, $d = 5{\cdot}1$ cm; ○, $d = 10{\cdot}2$ cm; □, $d = 15{\cdot}2$ cm; ◇, $d = 20{\cdot}3$ cm. $D = 30{\cdot}5$ cm, $Ra = 20{\cdot}4 \times 10^8$; ●, $d = 10{\cdot}2$ cm; ■, $d = 15{\cdot}2$ cm. $D = 15{\cdot}2$ cm; $Ra = 0{\cdot}86 \times 10^8$; ⊛, $d = 5{\cdot}1$ cm; +, $d = 10{\cdot}2$ cm; ×, $d = 15{\cdot}2$ cm.

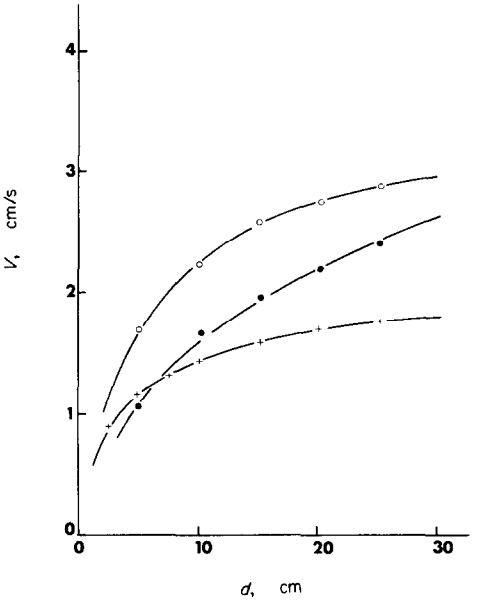

FIG. 13. Variation of centerline velocity in the plume with d. Data: ○, $D = 30{\cdot}5$ cm at $Ra = 6{\cdot}9 \times 10^8$; ●, $D = 30{\cdot}5$ cm at $Ra = 20{\cdot}4 \times 10^8$; +, $D = 15{\cdot}2$ cm at $Ra = 0{\cdot}86 \times 10^8$. $Q = 72{\cdot}4$, 318·0, 20·5 W respectively.

ment. The distributions at $d = 10{\cdot}2$, $15{\cdot}2$ and $20{\cdot}3$ cm are very similar in form to that calculated by Fujii [12] for a plume generated above by a point heat source. The plume rising from the smaller hemisphere behaves in a similar way.

The initial thickness of the velocity region is a consequence of the flow being concentrated in the boundary region adjacent to the hemisphere. The flow is primarily tangential near the surface. The tangential component gathers the fluid and narrows the flow field, while the fluid accelerates downstream, due to buoyancy. The combination of these two effects is the initial narrowing. As the flow becomes essentially vertical it approaches the characteristics of an axisymmetric plume. However, this plume would not be expected to initially have the flow and growth properties of one generated by a much more concentrated source. It would, therefore, be of interest to study the further downstream development of the flow to find if it does indeed eventually approach the characteristics of that generated by a concentrated source.

To assess this question, for the limited d range of our data, we have plotted the local maximum velocity V_{max} vs d in Fig. 13. It is seen to gradually approach a constant value downstream, which agrees with the predictions of the plume theory discussed below. The similar plot, at a higher heating rate, $Ra = 20{\cdot}4 \times 10^8$, shows lower values of V_{max} and a more rapid rate of increase. This is suggested by the distributions in Fig. 12 which are substantially thicker and very flat at the peak region. There is a general disagreement in the form of the distributions at the two heating rates.

Velocity profiles for the smaller hemisphere at $Ra = 0{\cdot}86 \times 10^8$, which corresponds to the same value of ΔT as that for the larger one at $Ra = 6{\cdot}9 \times 10^8$, are also shown in Fig. 12. The peak velocity V_{max} is found to be smaller and the velocity region diameter is smaller. Values of V_{max} plotted in Fig. 13 indicate that a constant value of V_{max} has almost been attained by $d = 25{\cdot}4$ cm.

The measured temperature profiles are shown in Fig. 14 as ϕ vs y, where $\phi = (t - t_\infty)/(t_0 - t_\infty)$, t_0 being the measured centerline temperature. These curves show a behavior very similar to that of the velocity field. The field narrows from $d = 5{\cdot}1$ cm to $d = 10{\cdot}2$ cm and then gradually thickens. The form of the curves is again similar to those of plume theory. Distributions at this same heating rate but with the insulator base, are very similar. The maximum velocity was a little lower and the flow field narrower. The temperature field is also found to be much thicker for the higher heating rate.

Another interesting characteristic of these transitional flows is seen in Fig. 15, where we have plotted the downstream centerline temperature $t_0 - t_\infty$ vs d for

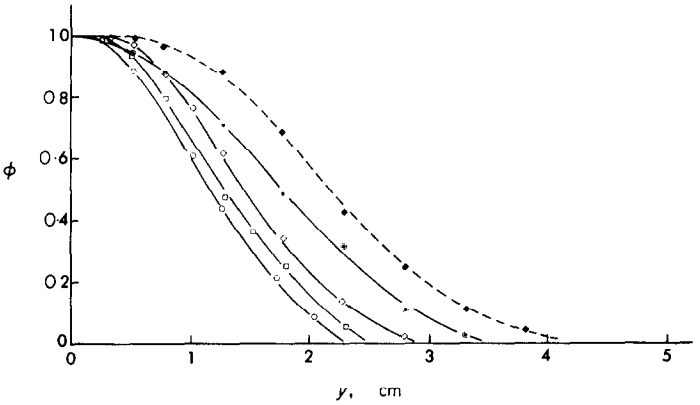

FIG. 14. Temperature distributions in plume flow above the upright hemisphere. $D = 30{\cdot}5$ cm, without base. Data: $Ra = 6{\cdot}9 \times 10^8$; ◉, $d = 5{\cdot}1$ cm; ○, $d = 10{\cdot}2$ cm; □, $d = 15{\cdot}2$ cm; ◇, $d = 20{\cdot}3$ cm. $Ra = 20{\cdot}4 \times 10^8$; ◆, $d = 20{\cdot}3$ cm.

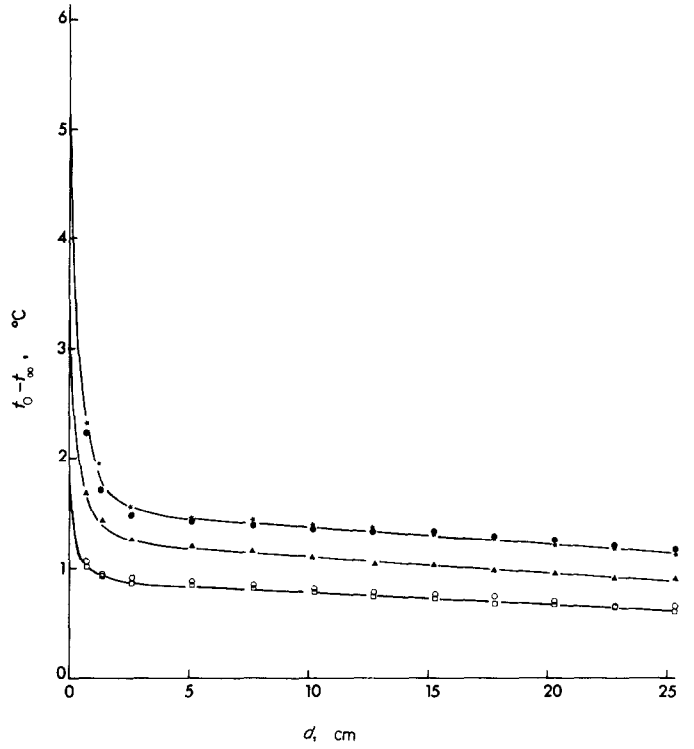

FIG. 15. Variation of centerline temperature in plume flow above the upright hemisphere. $D = 30{\cdot}5$ cm. Data: Without base; —— ○, $Ra = 6{\cdot}9 \times 10^8$; ●, $Ra = 20{\cdot}4 \times 10^8$. With insulator base; - — □, $Ra = 6{\cdot}9 \times 10^8$; ▲, $Ra = 13{\cdot}4 \times 10^8$; ★, $Ra = 20{\cdot}4 \times 10^8$.

the two upright configurations. The sharp drop in temperature immediately above the heated surface is in keeping with our earlier finding of a large surface heat transfer coefficient h at $\theta = 90°$. Thereafter, the centerline temperature decays very gradually with d. This data is for the hemisphere with an insulator base at Ra values of 6·9, 13·4 and $20{\cdot}4 \times 10^8$ and without the base at the two extreme values. The value of Q is certainly reflected in the wake temperature levels and the presence of the base has little effect.

We will now compare our measurements of the velocity and temperature in the shed plume with the theory of an axisymmetric plume above a point heat source. From the analysis of Fujii [12], the centerline velocity component V_{max} and temperature difference from ambient $(t_0 - t_\infty)$ are given, in terms of distance x above a concentrated source, as,

$$V_{max} = k_1(Pr)\left(\frac{g\beta}{2\pi\nu\rho C_p}\right)^{1/2} Q^{1/2} \tag{1}$$

$$t_0 - t_\infty = \frac{k_2(Pr)Q}{2\pi\nu\rho C_p x} \tag{2}$$

where Q is the rate of heat input by the source, ρ the density and C_p the specific heat of the fluid. The values of $k_1(Pr)$ and $k_2(Pr)$ are obtained from a numerical solution of the given equations. Values at several Pr are listed by Fujii [12]. We see that the centerline temperature is predicted to decrease downstream inversely with x. The velocity level remains unchanged. The analysis also predicts a thickening of the velocity and temperature regions as $x^{1/2}$ and a thinning according to $Q^{1/4}$. The rate of flow above the point source was also calculated and found to be independent of Q, varying linearly with x.

A comparison of our results with these predictions shows some surprising results. From Fig. 12, the velocity V_{max} has a lower value at the higher heating rate, contrary to equation (1). The velocity and thermal regions are found to be thicker at the higher heating rate, also in disagreement with the theory. This very different behavior must arise in the mechanisms which generate the shed plume, which are clearly very different from those of a concentrated source.

We saw, in Figs. 5 and 6, that the boundary-layer flow starts thickening rapidly at a lower value of θ for the higher heating rate. The flow has continued around the curved surface due to a favorable motion pressure gradient and in opposition to the normal buoyancy component. However, at higher heating rates the boundary-layer flow starts rising from the curved surface earlier, perhaps due to the higher momentum level. The upward flow region immediately above the hemisphere thus becomes thicker instead of thinner as predicted for a point source plume. Early separation also affects downstream thinning of the plume flow. Since the principal flow direction is tangential, it is closer to vertical for earlier separation, and has a relatively smaller horizontal component. The initial narrowing of the downstream flow, discussed earlier, is a consequence of this component and would, therefore, be less at the higher heating rate. Thus, both effects tend to broaden the shed-flow region at higher heating rates. Perhaps the decreasing spatial concentration of the shedding region, with increasing Q, also causes the lower velocity levels seen in Fig. 12. This does not mean lower total momentum, which would be an integral.

The consequences of these effects are clearer in Fig. 13 where V_{max} appears to approach to a constant value at very different rates in the three cases. For the small hemisphere ($Q = 20{\cdot}5$ W), an extrapolation suggests that a constant value would be reached at about three diameters downstream of the top of the hemisphere, i.e. at $d \approx 46$ cm.

For the large hemisphere, the equivalent distance downstream would be $d \approx 92$ cm. Since our tank was not this deep, we can only interpret the trends of the data. Unlike the curve for the small hemisphere, that for the large one and at the high heating rate, $Q = 318{\cdot}0$ W, V_{max} is still increasing rapidly at $d = 25{\cdot}4$ cm. The development of the shed flow toward concentrated-source plume characteristics is much slower, in terms of d. The lower heating rate, $Q = 72{\cdot}5$ W, with the large hemisphere, results in an intermediate rate of increase. However, it is very interesting that our results suggest that the middle curve, at highest Q, will cross the upper one, in accordance with equation (1). Another curious feature is seen in Fig. 12. The profiles are very flat near the centerline at the higher heating rate and not of the form calculated by Fujii [12], whereas those at lower Q are quite similar to the calculated ones. These effects are obvious consequences of the dependence of the separation mechanism on the heat input.

The temperature results in Fig. 15 agree with these interpretations. Note that the centerline temperature is higher at higher Q, resulting in greater buoyancy and a greater rate of increase in velocity V_{max}.

All of these observations are consistent with the reasonable expectation that the shed flow will ultimately be unaffected by starting effects, other than Q, and will rise as an axisymmetric plume having the characteristics of one arising from a concentrated source. This inference is further supported by a comparison of the velocity curves for $Q = 72{\cdot}5$ and $20{\cdot}5$ W. From equation (1), the predicted ratio of V_{max} is 1·88. The asymptotic values suggested by Fig. 13 are about this same ratio.

We have mentioned that the shed plume was found to be laminar. However, further downstream it becomes unstable to natural disturbances as do other buoyancy-induced flows. These disturbances amplify to lead the flow through transition to turbulence. Since the present measurements did now show any bursts, as found by Jaluria and Gebhart [13] in flows adjacent to heated vertical surfaces, we were apparently upstream of the beginning of transition.

However, at $Ra = 20{\cdot}4 \times 10^8$ for the larger hemisphere and at downstream locations around $d = 15{\cdot}2$ cm

and beyond, we did observe disturbances in our sensor outputs. Further upstream and at lower values of Ra, none were detected. The disturbances were close to sinusoidal and their amplitude increased downstream. Their amplitudes were only a few percent of the measured local peak velocity and temperature. Samples of the velocity disturbances are seen in Fig. 16. The form of the disturbance and its amplitude indicates that the flow is still laminar. These growing disturbances will presumably give rise to turbulent bursts, marking the onset of the transition regime.

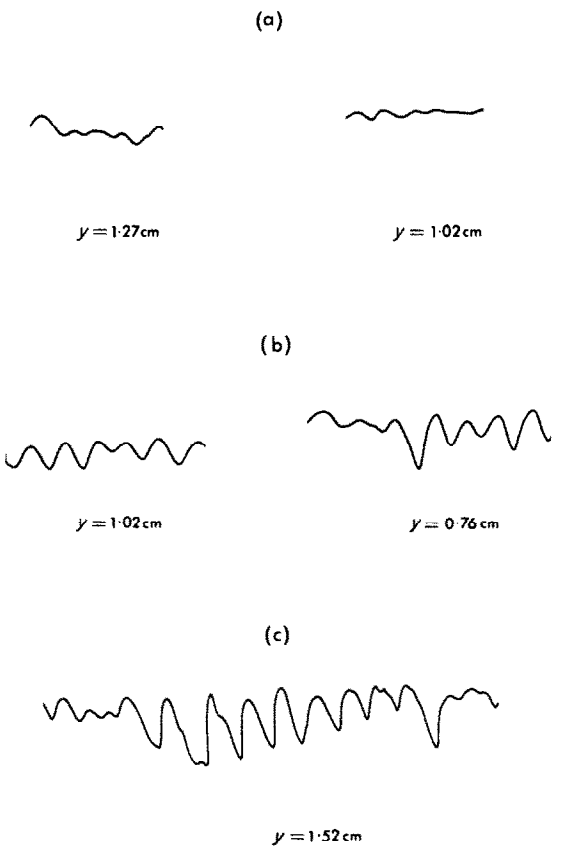

FIG. 16. Observed velocity disturbance in plume flow above the 30·5 cm diameter upright hemisphere at $Ra = 20{\cdot}4 \times 10^8$. Time scale is 5 s per horizontal division. Data: (a), $d = 15{\cdot}2$ cm; (b), $d = 20{\cdot}3$ cm; (c), $d = 25{\cdot}4$ cm.

The observed disturbance frequency was always around $\frac{1}{6}$ Hz. There have been no stability calculations for this transitional phase of the shed flow. However, one might relate the boundary region adjacent to the surface to that adjacent to a vertical surface. If the hemisphere is approximated as a vertical surface 15·2 cm high, at the same ΔT and in water, linear stability results, Gebhart [14], predict maximum amplification of disturbance components having frequencies of about 0·25 Hz. This, along with the downstream constancy of the observed frequency, seen in Fig. 16, suggest a frequency filtering mechanism similar to that found for many natural convection flows. All the disturbance profiles shown are at the same recorder sensitivity and it is seen that disturbance amplitude increases downstream. Obviously, data must be taken further downstream in the transition and turbulent regimes for a better understanding of the mechanism of transition of this flow.

4. *The inverted hemisphere*

Measurements were also taken in the flow shed above the upper edge of the inverted hemisphere. This flow is substantially different, particularly close to the trailing edge. Recall that the flat upward-facing base of the hemisphere is insulated and that no buoyant fluid is expected to rise from it. However, the detached boundary-layer fluid rises all around the edge of the base in a circular sheet. We recall that no unattached or reverse flow occurred over the upright hemisphere.

The measured velocity and temperature profiles at d values of 0·25, 1·78 and 5·6 cm, where d is the vertical distance above the trailing edge, are shown in Fig. 17. The horizontal distance y is measured from the vertical line through the trailing edge, $y = 0$. Positive values denote distances radially outward and negative ones inward toward the axis of the hemisphere. The profiles at $d = 0$ are not shown. They extend from $y = 0$ to positive y and are similar to those seen in Fig. 2 for the boundary region flow.

The profiles at $d = 0{\cdot}25$ cm are narrow, still of boundary region form, although they have begun to spread to negative y. In fact, some fluid has very rapidly rounded the edge. Note that already at $d = 0{\cdot}25$ cm appreciable velocity is found as far in as $y = -1{\cdot}0$ cm. This is clearly a large motion pressure effect. This indicates diffusion into the stagnant region above the base. At $d = 1{\cdot}78$ and 5·6 cm the shed flow shows a tremendous shift inward. The circular sheet of fluid is contracting rapidly toward the axis. It had concentrated momentum and thermal energy, upon separation from the heated surface. After the constraint of the surface is removed, at separation, the flow tends to rapidly entrain fluid on both sides. However, unless we postulate back-flow in the inner region, in disregard of the data of Fig. 17, there is no continuing entrainment on that side. The pressure in this region is, therefore, very low, due to the buoyancy and no opportunity to produce momentum. This is the cause of the quick turning of the separating boundary region flow just above $d = 0$. A study of the interaction of adjacent plane plumes, by Pera and Gebhart [15], shows a different mechanism when entrainment on the inner surfaces is also possible.

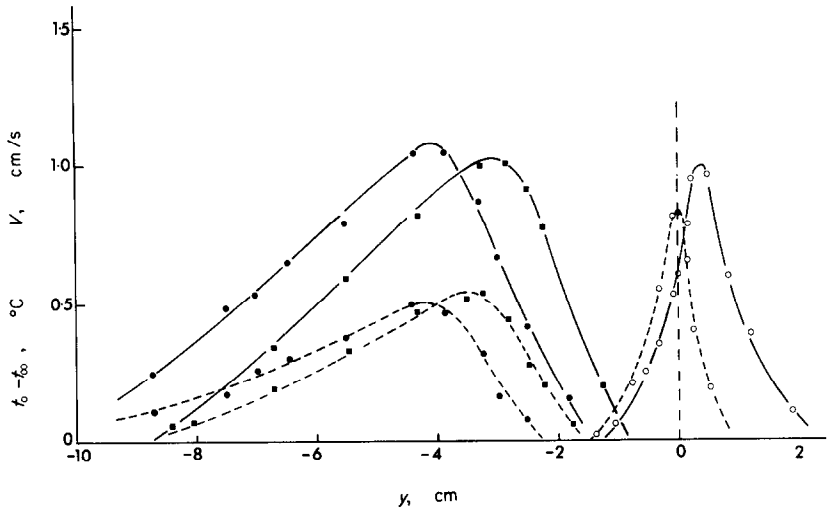

FIG. 17. Velocity and temperature distributions in the wake above the inverted hemisphere at $Ra = 6{\cdot}9 \times 10^8$. $D = 30{\cdot}5$ cm. ——, velocity and ----, temperature. Data: ○, $d = 0{\cdot}25$ cm; ■, $d = 1{\cdot}78$ cm; ●, $d = 5{\cdot}6$ cm.

Returning again to the contraction of the circular sheet of shed flow, the y locations of the peaks in the velocity and temperature distributions indicate an average inflow angle of around 30°, with the horizontal, up to $d = 1{\cdot}78$ cm. Thereafter, $d = 5{\cdot}6$ cm, the flow is essentially vertical. Therefore, the flow region periphery sharply decreases at small d and results in the substantial difference between the profiles at $d = 0{\cdot}25$ cm and at 1·78 cm. Still further downstream, the peak temperature decreases and the peak velocity increases very slightly. These are the expected results of entrainment and of the buoyancy force. Otherwise the profiles at $d = 1{\cdot}78$ and 5·6 cm are very similar in extent and form, indicating, as we have seen, an almost vertical flow in this d range.

Since the flow, at lower values of d, is at a small angle with the horizontal, and, since our y traverses are horizontal, the actual flow region thickness perpendicular to the flow direction is much less than that suggested by Fig. 17. Also, the periphery of the flow region decreases sharply with d. This would be expected to cause downstream thickening of the flow region. Recalling that the Q being convected upward is independent of d in any given flow, the spreading of the temperature region also results from this sharp decrease in periphery. Our measurements at a higher heating rate, $Ra = 15{\cdot}5 \times 10^8$, were very similar. A more detailed study is obviously needed to fully understand the mechanisms of this separation and of the resulting axisymmetric flow.

5. *Uniform surface heat flux condition*

The upright and inverted orientations were also studied for the surface subject to a uniform heat flux condition. We were interested in the variation of the surface temperature with θ. Since the heat flux q'' is uniform, the local surface temperature difference is inverse to the local heat-transfer coefficient h. We also investigated the shed plume flow for an upright and inclined orientation. Given the heater arrangement, the uniform surface temperature condition may be attained only when the axis of symmetry is vertical. The uniform flux condition may be imposed for any orientation.

The variation of the surface temperature excess over the ambient $t_0 - t_\infty$, with the downstream angular location θ is shown for both the upright and inverted configurations, in Fig. 18. For the former, with an insulator base, $t_0 - t_\infty$ initially increases with θ to a maximum value around $\theta = 60°$ and then decreases.

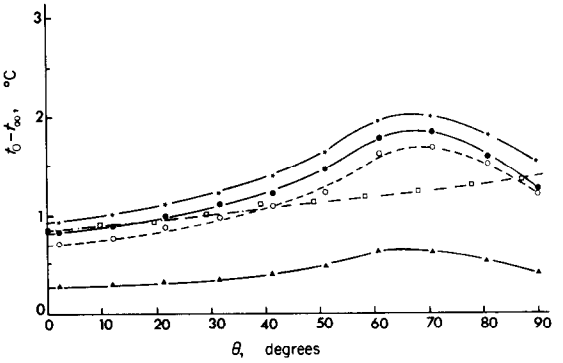

FIG. 18. Variation of surface temperature with θ for the uniform surface heat flux condition, $D = 30{\cdot}5$ cm. q'' values are in W/m². Data: ----, Upright hemisphere without base at $q'' = 198{\cdot}5$. —·—, Inverted hemisphere at $q'' = 198{\cdot}5$. ——, Upright hemisphere with base; ▲, $q'' = 45{\cdot}7$; ●, $q'' = 198{\cdot}5$; ★, $q'' = 238{\cdot}0$.

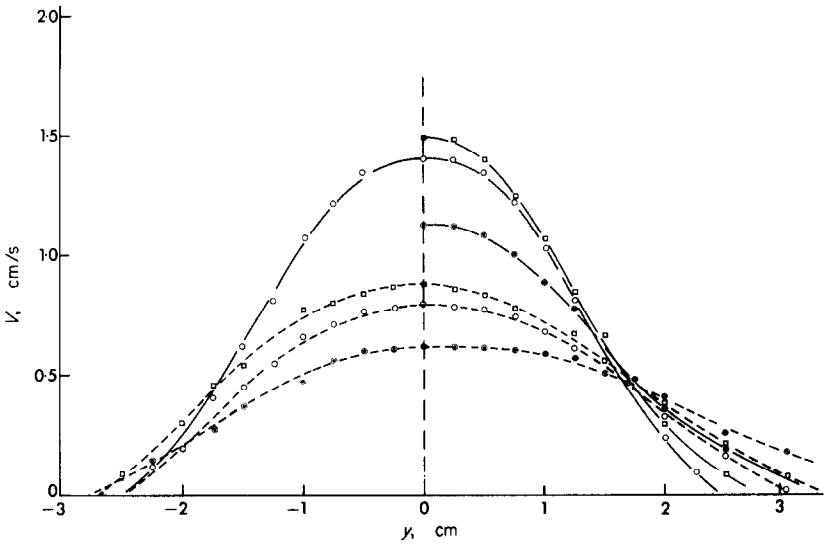

FIG. 19. Velocity distributions over the 15·2 cm hemisphere with uniform surface heat flux $q'' = 649{\cdot}0\ \mathrm{W/m^2}$. Data: ——, upright hemisphere; – – –, inclined hemisphere. ◉, $d = 5{\cdot}1$ cm; ○, $d = 10{\cdot}2$ cm; □, $d = 15{\cdot}2$ cm.

for each flux level. This implies a decrease of h to a minimum value and then a sharp increase to $\theta = 90°$, as found for a uniform temperature surface condition, Fig. 10. Without the base, lower values of $t_0 - t_\infty$ were measured. This indicates a higher h, also as found before. For the inverted hemisphere $t_0 - t_\infty$ is seen to increase monotonically to $\theta = 90°$ and the behavior of h is again similar to that with a uniform temperature condition.

The principal reason for this study with the uniform surface flux condition was to determine the consequences, on the shedding and plume behavior, of a non-symmetric upstream heating surface. For this purpose, the small hemisphere was used, at a flux level of $649{\cdot}0\ \mathrm{W/m^2}$. Measurements were made with its axis vertical and at an inclination of 15° with the vertical. Downstream velocity profiles are seen in Fig. 19. For the inclined arrangement, d is taken as the vertical distance from the top of the surface, at which point, y, perpendicular to d, is taken as zero. The axis of hemisphere symmetry tilts to the right in Fig. 19 and lies in the plane in which the probe traverses were made.

Inclination is seen to have a large effect in this downstream range. The plume has much greater cross-section and a much lower velocity level. The curves are also found to be very flat around $y = 0$. The flow is shifted to the right, consistent with the greater heat input on that side. The $t_0 - t_\infty$ distributions showed the same effects. The asymmetry is not very large and is seen to decay quite rapidly. It must also be noted that the traverse is in the direction of narrowest flow region, it being widest in the perpendicular direction. We see that tilting has sharply increased the flow area, with a compensating decrease in velocity level. Also, tilting changes the orientation of the buoyancy force with respect to the surface, particularly near the leading edge where the tangential component is decreased. This also tends to lower the velocity level.

Since the total heat input to the hemisphere was $Q = 23{\cdot}2$ W, the results for the axis vertical may be compared with those shown in Fig. 12, for the isothermal condition and $Q = 20{\cdot}5$ W. With uniform flux the flow region is thicker and the peak velocities are lower. This may be due to an earlier separation arising with the larger Q. The increase in surface temperature with θ, for the uniform flux case, may also be expected to cause an earlier separation since this implies increased buoyancy near the top of the hemisphere. Otherwise the results are very similar.

CONCLUSIONS

Our measurements of the velocity and temperature fields in the boundary-region flow adjacent to upright and inverted configurations indicate a thicker boundary region and higher flow velocities in the upright configuration at given downstream angular locations. This results quite reasonably from geometry and buoyancy considerations. The downstream variation of the boundary-layer thickness, the maximum velocity and the local heat-transfer coefficient h were determined for both flow configurations. Unlike the monotonic behavior found in the inverted orientation, for the upright one both the velocity and the boundary-layer thickness distributions showed rapid departure downstream from

their upstream trends of increase. A convection coefficient minimum was found. These events define a concept of "separation" in such a natural convection flow, consistent with the earlier study of Pera and Gebhart [11]. This separation is very different from the usual boundary-layer separation encountered in forced flows. There is no necessary flow reversal, flow unsteadiness, or external field of large pressure gradient.

The subsequent study of the mechanism of boundary-layer material shedding to form a downstream plume, in the upright configuration, yielded several important insights into very little understood processes. The measurements indicated an axisymmetric flow which appears to approach a constant velocity level downstream, as calculated for an axisymmetric plume above a concentrated heat source. The decay of the temperature field and the growth of the flow region were studied. Increasing heat input thickened the flow region and had the anomalous effect of a decrease in flow velocity level. This is thought to be related to both the growing angular region involved in separation and to the longer downstream distance required to adjust this more extensive flow to a condition more consistent with its free rise. Plume flow above an inclined hemisphere was asymmetric, as expected.

The wake rising above the edge of an inverted hemisphere, a body with an unheated and insulated upper face, contracted sharply toward the axis of symmetry. This resulted in a rapid increase in the flow region thickness downstream. The upright hemisphere orientation showed better heat transfer, at given ΔT, than the inverted one. Heat transfer was again worse when an extensive insulator base was placed underneath.

Our results are in reasonable agreement with existing theoretical and experimental studies for a sphere, where comparisons are realistic. Our flows were all laminar. However, amplifying natural disturbances were observed in the shed plume. Due to the size of the tank and positioning of the hemispheres, the water surface was only around 32 cm above the top of the hemisphere. One would need greater downstream distances to study later stages of destabilization and transition.

These results, though nominally limited to hemispheres, have given a clearer understanding of natural convection flows arising from incomplete heated bodies of appreciable extent and shedding buoyant material into an extensive medium. The effect of the buoyancy force orientation on flow over curved surfaces, the nature of flow near the top end of a heated body and the effects of the geometry on the buoyant flow over the body have been clarified. These mechanisms are of general importance for other shapes and interactions. Such problems are very common, though little studied to date.

Acknowledgement—The authors wish to acknowledge support for this research under National Science Foundation Grant GK 18529.

REFERENCES

1. W. S. Amato and C. Tien, Free convection heat transfer from isothermal spheres in water, *Int. J. Heat Mass Transfer* **15**, 327 (1972).
2. A. A. Kranse and J. Schenk, Thermal free convection from a solid sphere, *Appl. Sci. Res.* **A15**, 397 (1965).
3. G. Schutz, Natural convection mass-transfer measurements on spheres and horizontal cylinders by an electrochemical method, *Int. J. Heat Mass Transfer* **6**, 873 (1963).
4. F. H. Garner and R. B. Keey, Mass transfer from single solid spheres—I and II, *Chem. Engng Sci.* **9**, 119 and 218 (1958–59).
5. H. J. Merk and J. A. Prins, Thermal convection in laminar boundary layers I, II and III, *Appl. Sci. Res.* **A4**, 11, 195 and 207 (1953–54).
6. A. Acrivos, A theoretical analysis of laminar natural convection heat transfer to non-Newtonian fluids, *A.I.Ch.E. Jl* **6**, 584 (1960).
7. T. Chiang, A. Ossin and C. L. Tien, Laminar free convection from a sphere, *J. Heat Transfer* **86C**, 537 (1964).
8. W. H. Braun, S. Ostrach and J. E. Heighway, Free-convection similarity flows about two-dimensional and axisymmetric bodies with closed lower ends, *Int. J. Heat Mass Transfer* **2**, 121 (1961).
9. K. Hollasch, A survey of the literature, design, and experimental verification of a measurement scheme for external turbulent natural convection flow, M.S. Thesis, Cornell University (1970).
10. Y. Jaluria and B. Gebhart, An experimental study of non-linear disturbance behavior in natural convection, *J. Fluid Mech.* **61**, 337 (1973).
11. L. Pera and B. Gebhart, Experimental observations of wake formation over cylindrical surfaces in natural convection flows, *Int. J. Heat Mass Transfer* **15**, 177 (1972).
12. T. Fujii, Theory of the steady laminar natural convection above a horizontal line heat source and a point heat source, *Int. J. Heat Mass Transfer* **6**, 597 (1963).
13. Y. Jaluria and B. Gebhart, On transition mechanisms in vertical natural convection flow, *J. Fluid Mech.* To be published.
14. B. Gebhart, Instability, transition, and turbulence in buoyancy-induced flows, *Ann. Rev. Fluid Mech.* **5**, 213 (1973).
15. L. Pera and B. Gebhart, Plume flow interactions, *J. Fluid Mech.* To be published (1974).